#### **Research Article**

Muhammad Yahya Tahir, Tauqeer Ahmad, Muhammad Usman, Areena Fatima, Wenshuo Zhang, Zilin Gong, Abdullah A. Al-Kahtani, Ammar M. Tighezza, Bhargav Akkinepally\*, Dahoon Ahn\*, and Dongwhi Choi\*

# Electrochemically prepared ultrathin twodimensional graphitic nanosheets as cathodes for advanced Zn-based energy storage devices

https://doi.org/10.1515/ntrev-2023-0210 received November 29, 2023; accepted January 15, 2024

**Abstract:** Zinc-ion supercapacitors (ZISCs) exhibit great potential to store energy owing to the benefits of high power density and environmentally friendly features. However, solving the drawbacks of low specific energy and poor cyclic performance at high current rates is necessary. Thus, developing better cathode materials is a practical and efficient way to overcome these limitations. This work presents an encouraging design of two-dimensional (2D) graphite ultrathin nanosheets (GUNSs) as a cathode material for ZISCs. The experimental results show that

\* Corresponding author: Bhargav Akkinepally, School of Mechanical Engineering, Yeungnam University, Daehak-ro, Gyeongsan-si, Gyeongbuk-do 38541, South Korea, e-mail: bhargav@ynu.ac.kr

**Muhammad Yahya Tahir, Areena Fatima:** Department of Environmental Sciences, Government College University Faisalabad, Faisalabad, Pakistan

**Tauqeer Ahmad:** School of Mechanical Engineering, Yeungnam University, Daehak-ro, Gyeongsan-si, Gyeongbuk-do 38541, South Korea; Department of Chemical and Biological Engineering, University of Porto, Faculty of Engineering, Rua dr. Roberto Frias, 4200-465 Porto, Portugal **Muhammad Usman:** Department of Metallurgical and Materials Engineering, University of Porto, Faculty of Engineering, Rua dr. Roberto Frias, 4200-465 Porto, Portugal

Wenshuo Zhang: State Key Laboratory of Applied Organic Chemistry and Department of Chemistry, Lanzhou University, Lanzhou 730000, China Zilin Gong: State Key Laboratory of Applied Organic Chemistry and Department of Chemistry, Lanzhou University, Lanzhou 730000, China; School of Physical Science and Technology, Lanzhou University, Lanzhou 730000, China Abdullah A. Al-Kahtani, Ammar M. Tighezza: Chemistry Department, College of Science, King Saud University, Riyadh 11451, Saudi Arabia

the GUNSs-based cathode material exhibits a wide surface area and rapid charge transformation features. The 2D GUNS as a cathode was tested in three-electrode systems, and it provided an exceptionally high capacitance of 641 F/g at 1 A/g in an aqueous ZnSO<sub>4</sub> electrolyte, better than GUNS- $N_2$  (462 F/g at 1 A/g) and pristine graphite (225.8 F/g at 1 A/g). The 2D GUNS has a rate performance of 43.8% at a current density of 20 A/g, better than GUNS-N<sub>2</sub> (35.6%) and pristine graphite (8.4%) at the same conditions. Furthermore, a ZISC device was fabricated using GUNSs as cathode and Znfoil as anode with 1 M ZnSO<sub>4</sub> electrolyte (denoted as GUNSs// Zn). The as-fabricated GUNSs//Zn device exhibits an excellent capacitance of 182.5 F/g at 1 A/g with good capacitance retention of 97.2%, which is better than pristine graphite (94.6%), and nitrogen-doped GUNS (GUNS-N<sub>2</sub>) cathode (95.7%). In addition, the GUNSs//Zn device demonstrated an ultrahigh cyclic life of 10,000 cycles, and 96.76% of capacitance was maintained. Furthermore, the GUNSs//Zn device delivers a specific energy of 64.88 W h/kg at an ultrahigh specific power of 802.67 W/kg and can run a light-emitting diode for practical applications.

**Keywords:** graphite, 2D nanosheets, electrochemical exfoliation, zinc-ion supercapacitor

## 1 Introduction

To obtain benefits from renewable energy sources, high-performance energy storage and conversion technologies are required to save energy, such as supercapacitors, batteries, and fuel cells [1–3]. However, the actual practical use at the grid level of rechargeable lithium-ion batteries is hampered by their low specific power and short lifespan due to slow ion-transport kinetics *via* intercalation/deintercalation [4,5]. Despite the progress made in lithium-ion batteries, other metal-ion batteries have also been researched alongside, such as potassium and sodium ion batteries [6,7]. Even though lithium-ion batteries are widely used in electric

<sup>\*</sup> Corresponding author: Dahoon Ahn, Department of Mechanical System Design Engineering, Seoul National University of Science and Technology, 232 Gongneung-ro, Nowon-gu, Seoul, South Korea, e-mail: dhahn@seoultech.ac.kr

<sup>\*</sup> Corresponding author: Dongwhi Choi, Department of Mechanical Engineering (Integrated Engineering Program), Kyung Hee University, 1732 Deogyeong-daero, Yongin, Gyeonggi, 17104, South Korea, e-mail: dongwhi.choi@khu.ac.kr

cars and portable electronics, there is still a pressing need for innovative battery systems that have the advantages of high voltage, cost-effectiveness, safety, and environmental friendliness, such as bivalent metal ion batteries such as magnesium [8], calcium [9], and zinc ion batteries [10]. Recently, many researchers have focused on dual-ion batteries, where the battery reaction involves both cations and anions [11,12]. DIBs possess higher energy densities than mono and divalent ion batteries; however, the power densities of batteries are low. Metal-ion supercapacitors, like lithium, sodium, and potassium ion supercapacitors, may successfully compensate for the insufficient specific power of rechargeable batteries. However, the extreme reactivity of these metals (lithium, sodium, and potassium) produces dendrite-at metal anodes, and the flammability of organic electrolytes offers severe safety concerns [13,14]. Therefore, aqueous energy storage technologies have gained a lot of interest because of their strong ionic conductivity and excellent safety benefits. Thus, it is extremely desirable to design unique and advanced aqueous energy storage devices with features like good safety, excellent specific power, and specific energy [15]. Lately, aqueous zinc-ion supercapacitors (ZISCs) have been designed, owing primarily to their superiorities in terms of cost-effectiveness, high specific energy, and extended lifespan [16,17].

ZISCs have been identified as the most appealing energy storage candidates due to their ability to combine the benefits of supercapacitors and batteries [18]. ZISCs typically consist of an anode of battery type and a cathode of capacitor type [19]. The metallic Zn-based negative electrode (anode) exhibits an excellent theoretical capacity of 823 mA h/g as well as a low redox potential of -0.76 V, making it a good energy storage material with a fairly large voltage window [19]. The working principle of ZISCs involves fast deposition/stripping of the Zn ion in the anode, resulting in high specific energy, and fast adsorption/desorption of the Zn ion on the cathode, resulting in high specific power [20].

Carbon-based materials have been the subject of much investigation for supercapacitors [21]. Carbon-based materials, including graphite, are becoming a new class of electrodes for supercapacitor systems due to their portability, excellent flexibility, easy fabrication methods, and outstanding electrical conductivity [22]. However, owing to its limited surface area, graphite foil exhibits a low specific capacitance. Its surface area might be enhanced *via* electrochemical exfoliation [23]. In high voltage, ions intercalate and transform into different gaseous species in the graphite layers in an electrolyte. The electrochemical

exfoliation process expands the surface area. Although electrochemically exfoliated graphite foil has been used in several research reactors, the method is difficult and challenging to implement on intact systems [24,25].

Herein, we present an encouraging cathode design of two-dimensional (2D) graphite ultrathin nanosheets (GUNSs) for ZISCs. The experimental results show that the GUNS-based cathode material exhibits a wide surface area and rapid charge transport. GUNS exhibits a high capacitance of 641 F/g at 1 A/g, outperforming GUNS-N<sub>2</sub> (462 F/g at 1 A/g) and pristine graphite (225.8 F/g at 1 A/g). GUNS has a good rate performance of 43.8% at 20 A/g, which is significantly higher than GUNS-N<sub>2</sub> (35.6%) and pristine graphite (8.4%) in the same conditions. The resulting ZISC device (GUNSs//Zn) demonstrates an excellent capacitance (182.5 F/g at 1 A/g). Further, the GUNSs//Zn demonstrate an ultrahigh cyclic life of 10,000 cycles, and 96.76% of capacitance was maintained. Furthermore, GUNSs//Zn reveals a specific energy of 64.88 W h/kg at an ultrahigh specific power of 802.67 W/kg.

# 2 Materials and methods

# 2.1 Synthesis of 2D GUNSs

Carbon paper served as an electrode for the preparation of 2D GUNSs. A silver pad was used to attach the carbon to a tungsten wire, and it was then added to the solution as a negative electrode. The single carbon paper was submerged in the solution. With a 5 cm distance between them, a platinum plate was positioned side by side with carbon paper. About 5 g of sulfuric acid (H2SO4, Sigma-Aldrich: 98% concentration) was diluted in 100 mL of deionized water to obtain the ionic solution. The electrochemical exfoliation process was performed using an electrode made of carbon paper and a DC bias voltage. A 5 V is applied to the electrode and left undisturbed for 30 min to obtain a mixed solution. Add 100 mL of deionized water to the solution and stir well. The exfoliated carbon was filtered via a 100 nm membrane with deionized water to generate a 2D GUNS solution. After that, 2D GUNS was sonicated using a mild water bath for 5 min to disperse them in a dimethyl formamide (DMF) solution. The suspension was centrifuged at 2,500 rpm to eliminate undesired large particles created during the exfoliation. The centrifuged suspension can then be used for film production and further characterization. These electrochemical exfoliations were all carried out at ambient temperature.

## 2.2 Physical characterization

The material's morphology was studied using a field emission scanning electron microscope (FESEM, HITACHI SU8220), a transmission electron microscope (TEM, FEI Themis Z), and an energy-dispersive X-ray spectrometer. To analyze crystal structure, an X-ray diffractometer (XRD, X'Pert Pro Analytical) by means of monochromatic radiations (Cu-Kα; = 0.15406 nm) was used. The elemental composition of 2D GUNS was studied using X-ray photoelectron spectroscopy (XPS).

#### 2.3 Electrochemical characterization

For the fabrication of the ZISC device, to design the positive electrode (cathode), the active substance, conductive carbon black, and polyvinylidene fluoride were combined in the ratio of 80:10:10 (wt%). The pulp mixture was mixed with N-methyl-2-pyrrolidone (NMP), pasted onto a carbon cloth (CC) of  $1 \times 1$  cm<sup>2</sup> surface, and dried for 6 h. About 1.2 mg/cm<sup>2</sup> of active material was bulk-loaded onto the CC. The negative electrode (anode) was a Zn plate with 1 M ZnSO<sub>4</sub> aqueous solution. The galvanostatic charge-discharge (GCD) and cyclic voltammogram (CV) were measured using an electrochemical workstation (CHI 660E, China). The CVs were performed in a voltage window varied from 0 to 1.6 V, while the GCD testing was performed at 1-10 A/g.

#### 2.4 Calculations

According to the discharge time, calculate the specific capacitance of the single electrode device and apply equation (1):

$$C = \frac{I\Delta t}{m\Delta V},\tag{1}$$

where C (F/g) is the gravimetric specific capacitance, I (A) is the applied current, m (g) is the mass of the active materials,  $\Delta V$  (V) is the potential window, and  $\Delta t$  (s) is the discharge time.

In a two-electrode system, the optimal mass ratio of the positive electrode and the negative electrode can be calculated according to equation (2):

$$\frac{m_+}{m_-} = \frac{C_- \Delta V_-}{C_+ \Delta V_+},\tag{2}$$

where  $m_+$ ,  $m_-$ ,  $C_+$ ,  $C_-$ , and  $\Delta V_+$ ,  $\Delta V_-$  are the masses, the specific capacitances, and the potential windows of the positive and negative electrodes, respectively.

The ZISC device's capacitance  $C_d$  (F/g), specific power (P) (W/kg), and specific energy (E) (W h/kg) are all computed as follows:

$$C_{\rm d} = \frac{I\Delta t_{\rm d}}{M \times (V)},\tag{3}$$

$$E = \frac{1}{2}C_{\rm d}V^2 \times \frac{1,000}{3,600},\tag{4}$$

$$P = \frac{E}{\Lambda t},\tag{5}$$

where  $\Delta t$  (s) denotes the discharge time, I (A) denotes the current, M (g) shows the mass of both the anode and the cathode, and V(V) represents the voltage window.

## 3 Results and discussion

The sample was synthesized using an electrochemical exfoliation technique, making use of carbon paper (working electrode), platinum foil (counter electrode), and Ag/AgCl (reference electrode) in H<sub>2</sub>SO<sub>4</sub>. Figure 1 shows a schematic illustration of the technique for fabricating the 2D GUNS.

Figure 2a-c illustrates the low- and high-resolution FESEM images of 2D GUNS. All images exhibit crumpled and ultrathin nanosheets overlapped and randomly arranged and supported by the high-resolution FESEM image (Figure 2c). The morphology of the prepared sample is quite similar to that of already reported materials [26]. The geometrical characteristics of the 2D GUNSs and the extent of exfoliation can be seen by TEM images. Figure 2d-f displays TEM images of as-prepared 2D GUNSs. Lowresolution TEM image shows ultrathin sheet-like morphology of 2D GUNSs (Figure 2d), and tiny pores can be observed (marked with circles). Furthermore, the highresolution TEM images (Figure 2e and f) exhibit that the porous graphite nanosheets consisted of four to six films and show a 0.3397 nm spacing, which is compatible with the (002) plane of graphite. Obviously, the elevated reactivity will provide the GUNSs with increased Zn ion storage. Additionally, the shorter ion transport route of porous GUNSs will help to enhance rate performance.

The XRD image of 2D GUNS is depicted in Figure 3a. Two characteristics of carbon diffraction reflexes were discovered, including (002) and (101). The presence of a distinct diffraction peak (002) at 26.6° in 2D GUNSs provides evidence that this material is a kind of graphite [27]. The peak location of 2D GUNSs is identical to that of natural graphite, as described in the literature. Since carbon is the fundamental ingredient, the crystal layer of carbon is unaffected by the electrochemical exfoliation process [28]. In

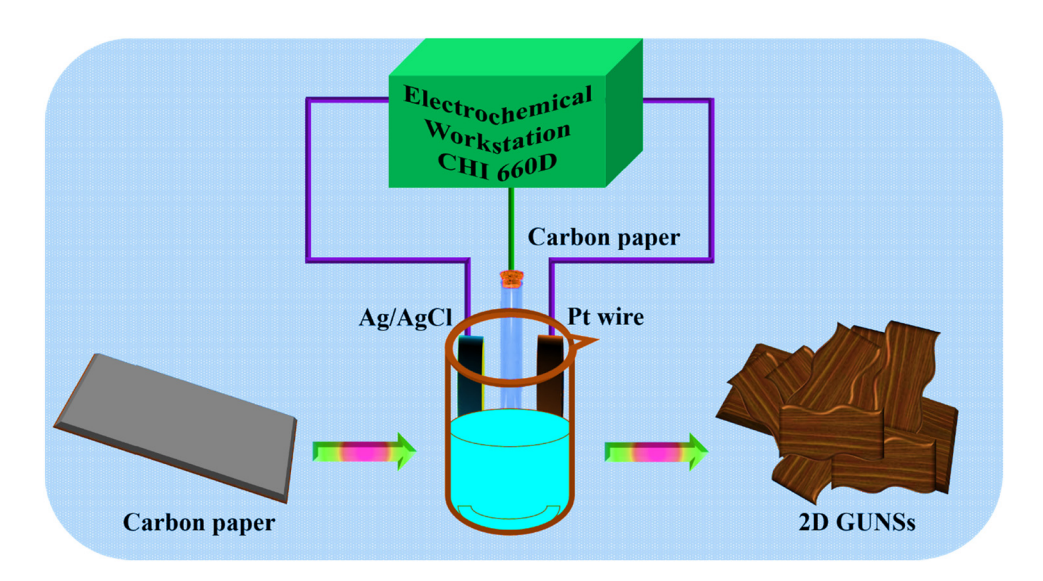


Figure 1: Schematic depiction of fabrication procedure of 2D GUNSs.

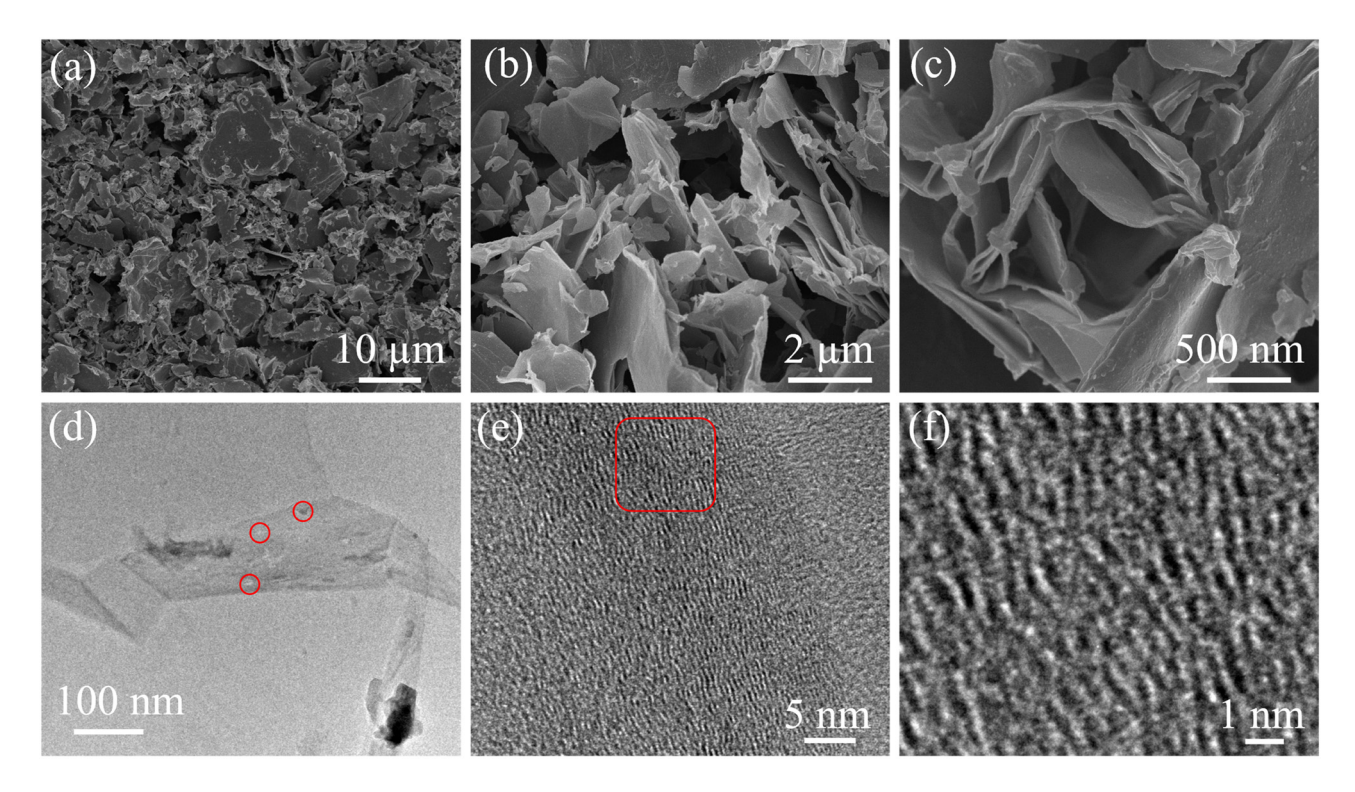
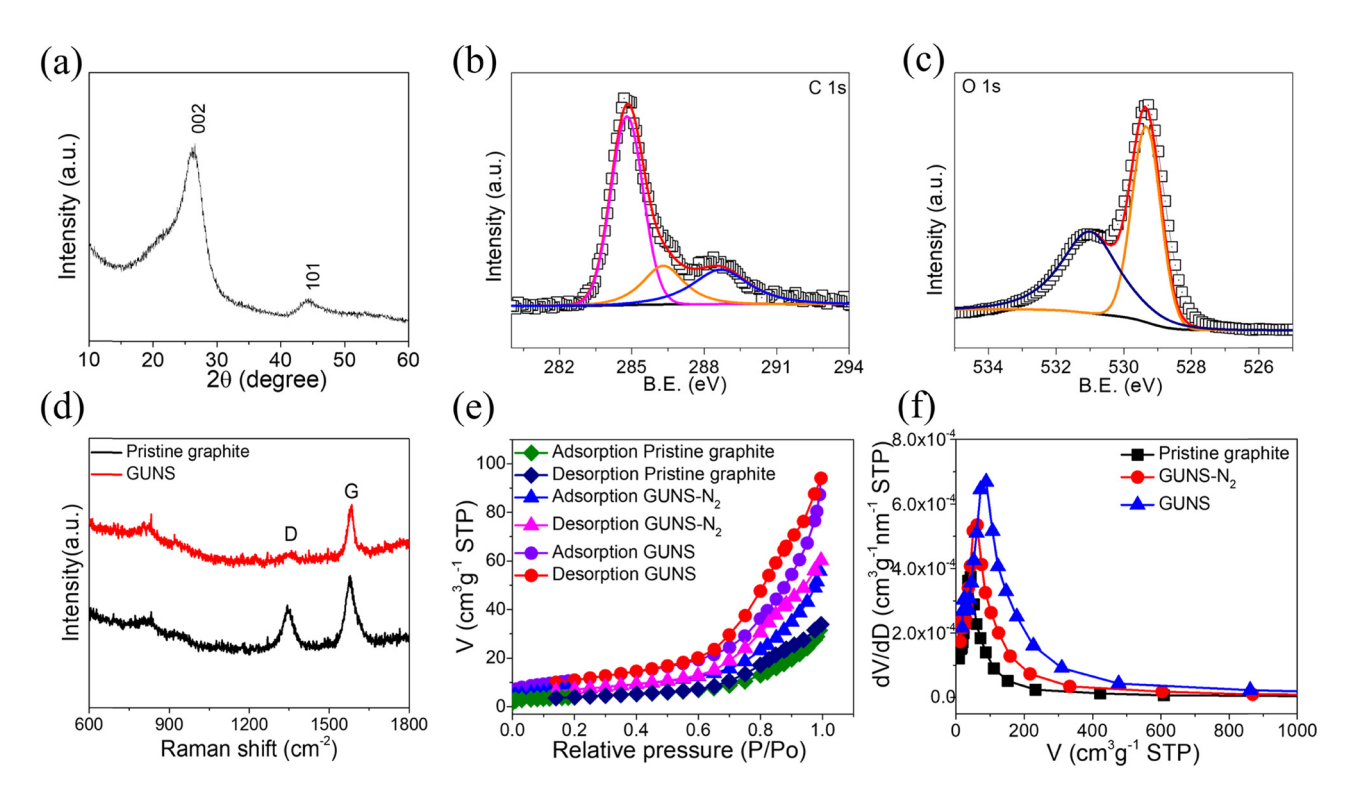


Figure 2: (a-c) Low- and high-resolution SEM images of 2D GUNSs, (d and e) low- and high-resolution TEM images of 2D GUNSs, and (f) HR-TEM image of 2D GUNSs.

addition, the XRD of carbon paper and GUNS were further analyzed. As shown in Figure S1, we found that the position corresponding to the peak of the characteristic peak (002) of carbon before and after the exfoliation process does not shift, but the width of the peak increases. This is due to the formation of bulky 2D ultra-thin graphene nanosheets after exfoliation by electrochemical means, which form

many voids during the nanosheet stacking process, thus increasing the spacing of the graphene nanosheets, resulting in a decrease in the crystallinity of the sample. In addition, the peak corresponding to the (101) crystal plane is shifted to the left, which proves the increase in crystal plane spacing.

Figure 3b displays a C-1s XPS spectrum of the 2D GUNSs obtained using XPS to study the existence of oxide defects.



**Figure 3:** (a) XRD patterns of 2D GUNSs, (b) C-1s XPS spectrum of 2D GUNSs, (c) O-1s XPS spectrum of 2D GUNSs, (d) the Raman spectra of the pristine graphite and 2D GUNSs, and (e and f) N<sub>2</sub> adsorption/desorption isotherms and pore-size distribution curve.

A dominating peak at 284.7 eV can be associated with (C-C) graphitic carbon. The deconvolution of the spectra showed the presence of many minor peaks with higher binding energies along with the C-C peak. Such characteristic peaks belong to oxides (284.6 eV belongs to C=C and 288.6 eV belongs to C=O) covalently bound extending to graphite in the case of an oxidized graphite. It is also possible that these peaks are due to solvent molecules that are still present inside the 2D GUNSs. Further, Figure 3c exhibits the O-1s XPS spectrum, which reveals two major peaks at 529.4 eV, ascribed to lattice oxygen, and 531.1 eV, ascribed to chemisorbed oxygen, respectively [29]. Therefore, the exceptional characteristics of the 2D GUNSs generated by high shear exfoliation were supported by XPS results, which are advantageous to enhancing the pseudocapacitive performance.

As shown in Figure 3d, we tested the Raman spectra of raw graphite and GUNS. It was observed that the G-band of the two samples remained unchanged. Compared to the original graphite, the peaks in the D-band of the GUNS were significantly reduced after electrochemical dissection, and the  $I_{\rm D}/I_{\rm G}$  value decreased from 0.61 to 0.22. This is attributed to electrochemical peeling, leading to many chemical bond breaks [30].

Specific surface area, porosity, and average pore diameter significantly affect the properties of ZHSC's electrode

material. As shown in Figure 3e, N<sub>2</sub> adsorption-desorption measurements were investigated for the textural properties of GUNS. Rapid uptake at high relative pressure was identified as the isotherm type IV with an H<sub>3</sub> hysteresis loop, which is relevant to mesoporous-like materials [31]. Distinctive hysteresis loop from 0.0 to  $1.0 P/P_0$  belongs to the typical Langmuir IV isotherms. The results show that GUNS has the largest BET-specific surface area of up to 59.8 m<sup>2</sup>/g, which is particularly suitable for energy storage applications due to GUNS-N<sub>2</sub> and pristine graphite samples. Due to the large specific surface area, it can promote electrolyte ion diffusion, enhance charge transport, and provide more electroactive sites for fast energy storage. The corresponding pore size distribution (Figure 3f) calculated by the Barrett-Joyner-Halenda method from the desorption branch further confirms the characteristics of the mesoporous structure. The pore size of the GUNS rises sharply at 107.6 nm, which marks a layered mesoporous feature. This porosity is mainly due to multiple inclined intermediate pores, which enhance the mass transport of GUNS and improve the utilization of the active surface area of the electrode.

In a three-electrode system, the electrochemical performance of pristine graphite, GUNS, and GUNS- $N_2$  was studied under a voltage window of -0.2 to 0.8 V using 1 M ZnSO<sub>4</sub> aqueous solution as the electrolyte. Figure 4a shows

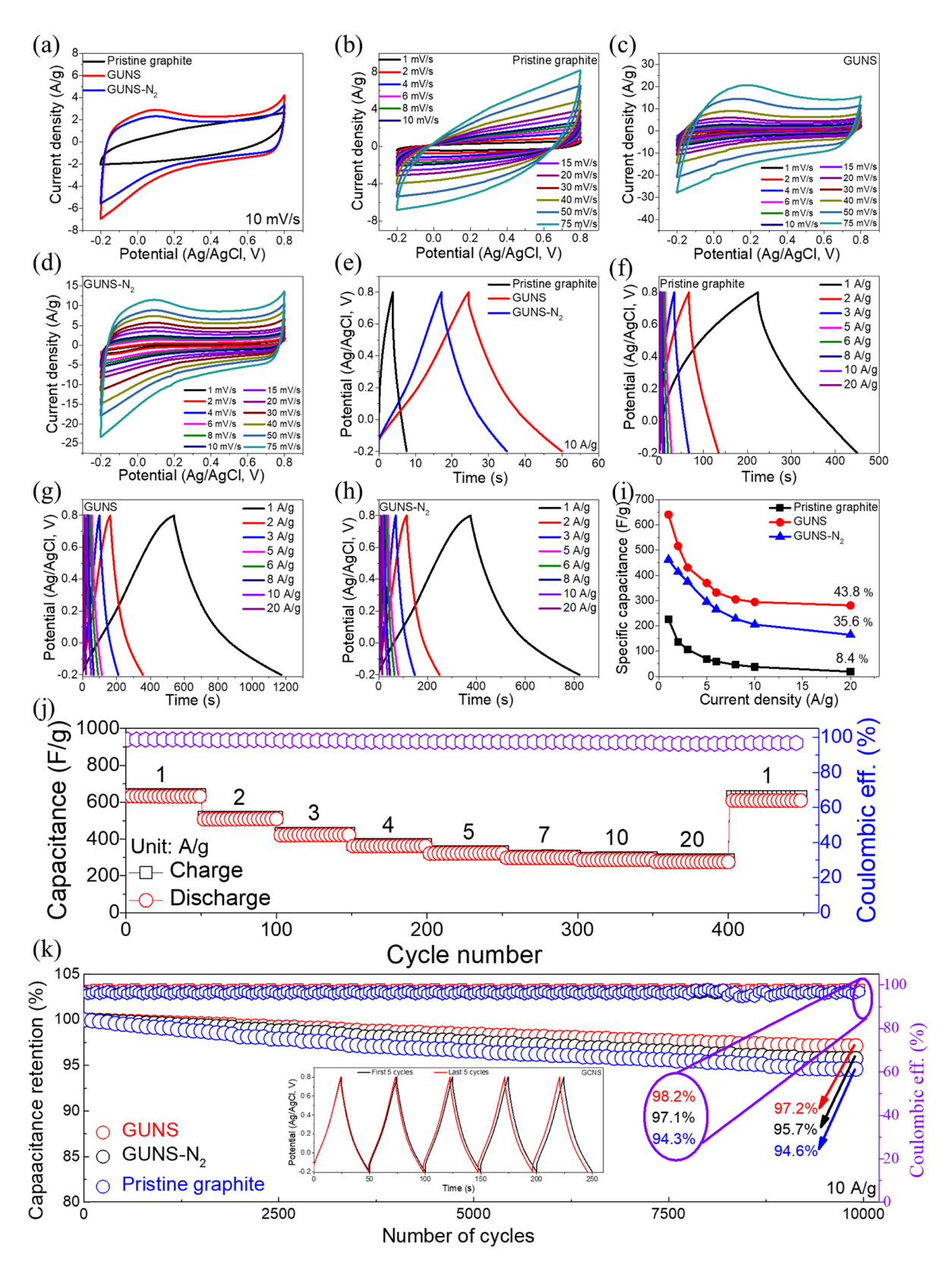


**Figure 4:** (a) Comparative CV curves of pristine graphite, GUNS, and GUNS- $N_2$  in potentials window of -0.2 to 0.8 V at 10 mV/s; CV curves at various scan rates for (b) pristine graphite, (c) GUNS, and (d) GUNS- $N_2$ . (e) Comparative GCD curves of pristine graphite, GUNS, and GUNS- $N_2$  electrodes. (f–h) GCD curves at various current densities range for pristine graphite, GUNS, and GUNS- $N_2$  electrodes. (i) Specific capacitance as a function of current density. (j) Rate capability and Coulombic efficiency *versus* the number of cycles up to 450 cycles of GUNS electrode. (k) Capacitance retention concerning cycles up to 5,000 cycles for pristine graphite, GUNS, and GUNS- $N_2$  electrodes (insets are first and last five cycles in 1 M ZnSO<sub>4</sub> electrolyte).

the CV curves of pristine graphite, GUNS, and GUNS-N<sub>2</sub> at a scan rate of 10 mV/s with a pair of redox peaks of GUNS and GUNS-N2. The GUNS obtained by electrochemical exfoliation has a large specific surface area, providing more active sites for zinc ions and promoting redox reaction. After N<sub>2</sub> treatment, the abundant oxygen-containing functional groups on the surface disappeared, decreasing the number of surface-active sites. As a result, the electrochemical performance is reduced. For further investigation, the CV curves are recorded at different scan rates (1-75 mV/s), as shown in Figure 4b-d. The shape of the CV curves of the electrodes remained stable as the scanning rates increased. indicating rapid mass transfer at the electrode/electrolyte interface. At different scan rates, GUNS electrodes have a larger area under the CV curve and greater charge storage capacity. In Figure 4e, the GCD curves of the pristine graphite, GUNS, and GUNS-N2 electrodes were compared at a current density of 10 A/g (potential window of -0.2 to 0.8 V). The GCDS electrode was observed to have a longer discharge time than the Ti<sub>3</sub>C<sub>2</sub>T<sub>x</sub> electrode, indicating higher charge storage capacity, which is consistent with the CV curves. Furthermore, GCD curves were recorded at different current densities from 1 to 20 A/g for pristine graphite, GUNS, and GUNS-N<sub>2</sub> electrodes (Figure 4f-h). The quasi-triangular GCD curve of the pristine graphite, GUNS, and GUNS-N<sub>2</sub> electrodes with high symmetry indicate high coulombic efficiency and excellent redox reaction reversibility. As shown in Figure 4i, the specific capacitance of the GCD curves for the three electrodes was also calculated. At a current density of 1 A/g, the GUNS electrode produces an ultra-high capacitance of 641 F/g, significantly larger than the GUNS-N<sub>2</sub> (462 F/g at 1 A/g), and pristine graphite (225.8 F/g at 1 A/g) electrode. After the current density is increased to 20 A/g, the specific capacitance generated by the GUNS electrode decreases to 280.8 F/g, and the initial capacitance retention rate is about 43.8%, which is much larger than that of GUNS-N<sub>2</sub> (35.6%) and pristine graphite (8.4%) electrodes, indicating that the GUNS electrode has good rate performance. This is attributed to increased specific surface area after exfoliation and the production of abundant oxygen-containing functional groups. After nitrogen treatment, the electrochemical performance decreases due to decreased surface oxygen-containing functional group content. Compared to GUNS, the specific capacitance and capacitance retention ratio of GUNS-N2 are reduced. Figure 4j shows the rate performance of the GUNS, with the specific capacitance values of 641, 517, 431, 370, 330, 304, 294, and 280 F/g at 1, 2, 3, 5, 6, 8, 10, and 20 A/g, respectively. When the current density is reduced to 1 A/g, a high discharge capacitance of 609.5 F/g can be recovered with a coulomb efficiency of up to 96.75%, demonstrating good electrochemical reversibility

and fast reaction kinetics. As shown in Figure 4k, the GUNS electrode exhibited exceptional cycle stability after 5,000 GCD cycles, with a capacitance retention rate of 97.2%, compared to the pristine graphite electrode (94.6%) and GUNS-N<sub>2</sub> electrode (95.7%). The coulombic efficiency of GUNS is as high as 98.2%, which is better than GUNS-N2 (97.1%) and pristine graphene (94.3%). The illustration in Figure 4k shows a comparison of the first and the last 6 GCD curves.

Furthermore, we performed XRD and SEM tests on samples before and after the electrochemical reaction. The test results show that the peak of XRD shifts to the left after the electrochemical reaction due to the insertion of Zn-ions. The strength of the peak is significantly weakened, which is attributed to the electrochemical reaction reducing the material's crystallinity. In addition, according to the comparison of SEM images before and after the reaction, the sample's morphology remained stable, proving that it had superior electrochemical stability. However, some crystals appeared on the sample's surface after the reaction, which was attributed to the precipitation of the electrolyte and recrystallization on the electrode surface (Figure S3).

We analyzed the XPS of different samples, and the C-1s spectrum showed a decrease in C=0, proving that the content of oxygen-containing functional groups was reduced (Figure S2). The SEM mapping of GUNS and GUNS-N2 was performed to demonstrate nitrogen functionalization, which reduces oxygen-containing functional groups, and these findings are consistent with XPS analysis (Figure S4(a) and (b)).

To further analyze the storage mechanism of Zn-ions, we performed ex situ XRD and TEM tests. As shown in Figure 5a, the peaks of the (002) crystal plane and (101) crystal plane of GUNS are shifted to the left after charging, proving that the crystal plane spacing has become larger, which is attributed to the insertion of Zn ions resulting in a wider lattice structure. In addition, the ex situ TEM test was also performed, and the crystal plane spacing was expanded to 0.362 nm after the end of charging (002), which proved the successful insertion of Zn ions. After the discharge, the crystal plane spacing became 0.346 nm, proving that the Zn ions were successfully inserted.

To examine the feasibility of the 2D GUNSs electrode for real-world practical applications, an aqueous GUNSs// Zn device was designed. Figure 6a depicts the CVs of GUNSs//Zn devices at different scan rates (4-75 mV/s). The approximately rectangular CV profiles supported the electrochemical double-layer approach. Even at high scan rates, the nearly rectangular-shaped CV profiles reveal the GUNSs//Zn device's fast kinetics, extremely reversible characteristics, and excellent rate performance [24]. Across

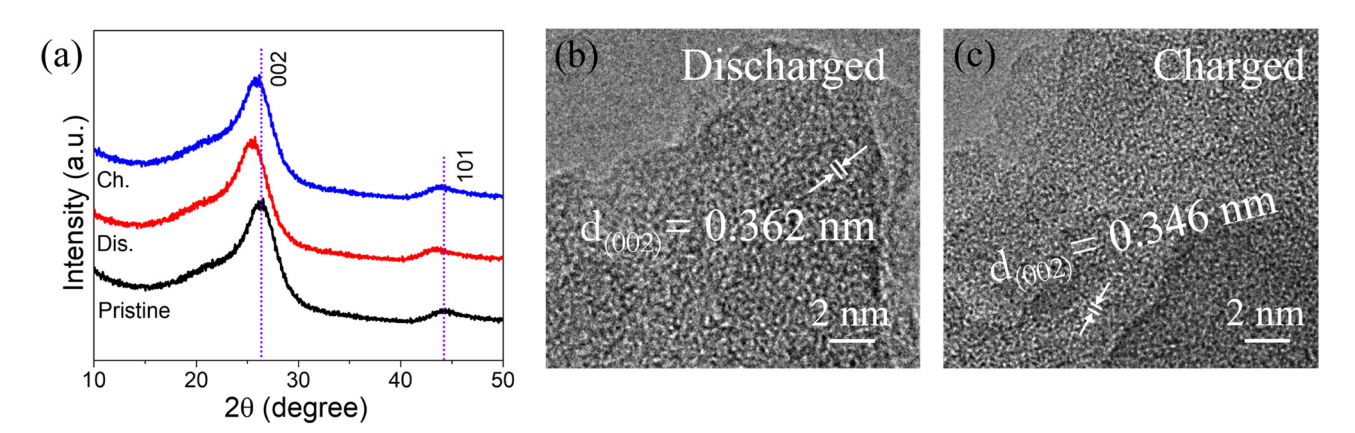
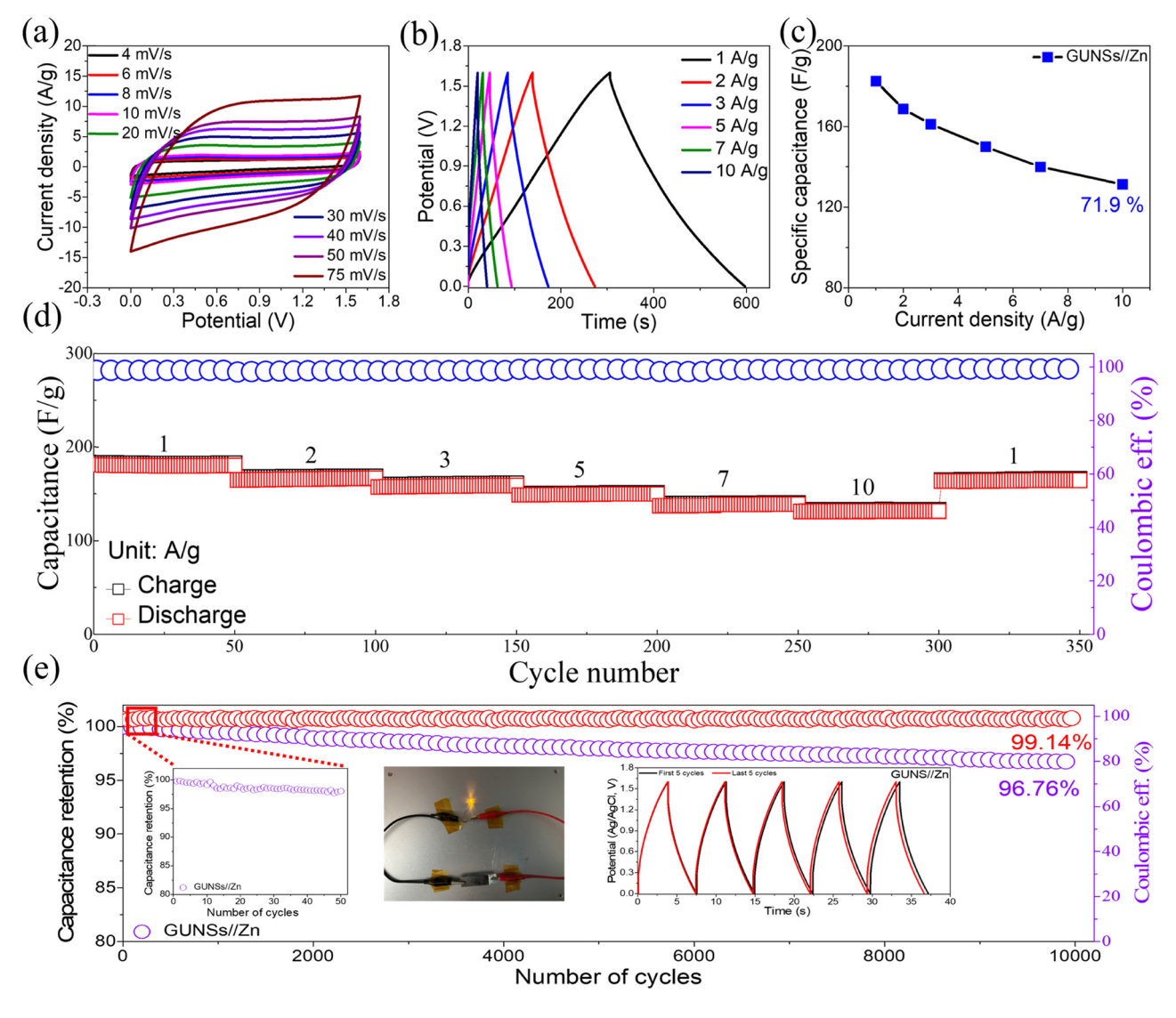


Figure 5: (a) Ex situ XRD of charge and discharge with GUNS. (b and c) HR-TEM images at discharge and charge.



**Figure 6:** Electrochemical characterization of GUNSs//Zn device: (a) CVs, (b) GCDs, and (c) capacitance *vs* current density. (d) Rate capability and Coulombic efficiency *versus* the number of cycles up to 350 cycles of GUNSs//Zn device. (e) Cycling stability (insets are first and last five cycles in 1 M ZnSO<sub>4</sub> electrolyte).

the porous surface, the electrolyte ions go through reversible absorption and desorption processes. Further, the GCD profiles of the GUNSs//Zn device at various current densities (1-10 A/g) are displayed in Figure 6b. The linear curve and symmetry revealed that the GUNSs//Zn device exhibited almost ideal behavior. With the decreasing current density, charge/discharge time increased. There is a little drop in potential, which is attributable to micropores that allow for fast electron and ion exchanges [32]. The specific capacitance (C<sub>d</sub>) of the GUNSs//Zn device has been computed using equation (1) and is shown in Figure 6c. The  $C_{\rm d}$  values of GUNSs//Zn device values are 182.5, 168.75, 161.25, 150, 140, and 131.25 F/g at 1, 2, 3, 5, 7, and 10 A/g, respectively. GUNSs//Zn device maintained 71.9% of its capacitance even at 10 A/g. GUNSs//Zn device has excellent stability, with coulomb efficiency remaining at 99.2% after 350 cycles at different current densities (Figure 6d). In addition, the cycling stability of the GUNSs//Zn devices over 10,000 cycles of GCD was studied, and the results showed that 96.76% capacitance and 99.14% coulombic efficiency were maintained, showing superior performance (Figure 6e). The inset of Figure 6e compares the first and last six cycles of GCD curves of GUNS//Zn. For practical applications, one GUNS//Zn device can light one light-emitting diode (LED); a digital photograph of lighting the LED is shown in the inset of Figure 6e.

Electrochemically active surface areas of the catalysts were calculated based on the double-layer capacitance ( $C_{\rm dl}$ ), which was obtained from cyclic voltammetry (CV) [33]. As shown in Figure S5, the  $C_{\rm dl}$  value of GUNS//Zn is determined to be 132 F/g.

Moreover, the charge storage method of GUNSs//Zn was investigated by analyzing the electrochemical kinetics using power law [34]

$$i(V) = a \cdot v^b, \tag{6}$$

$$\log(i) = b\log(v) + \log(a). \tag{7}$$

In the above equations, v indicates scan rate, i indicates peak current density, and a indicates arbitrary constants. The most significant component is the b-value, which describes the charge storage behavior (if the b-value is equal to 0.5, the charge storage mechanism is diffusion-controlled; if the b-value is equal to 1, the charge storage mechanism is capacitive). The b-values were calculated using the slope of equation (5) [log(v) vs log(i)], and equal to 0.81 and 0.85, respectively (Figure 7a), that is approaching 1, showing the hybrid nature of charge storage, such as capacitive- and diffusion-controlled leads to high electrochemical performance [35]. The typical capacitive- and diffusion-controlled contributions were determined as follows:

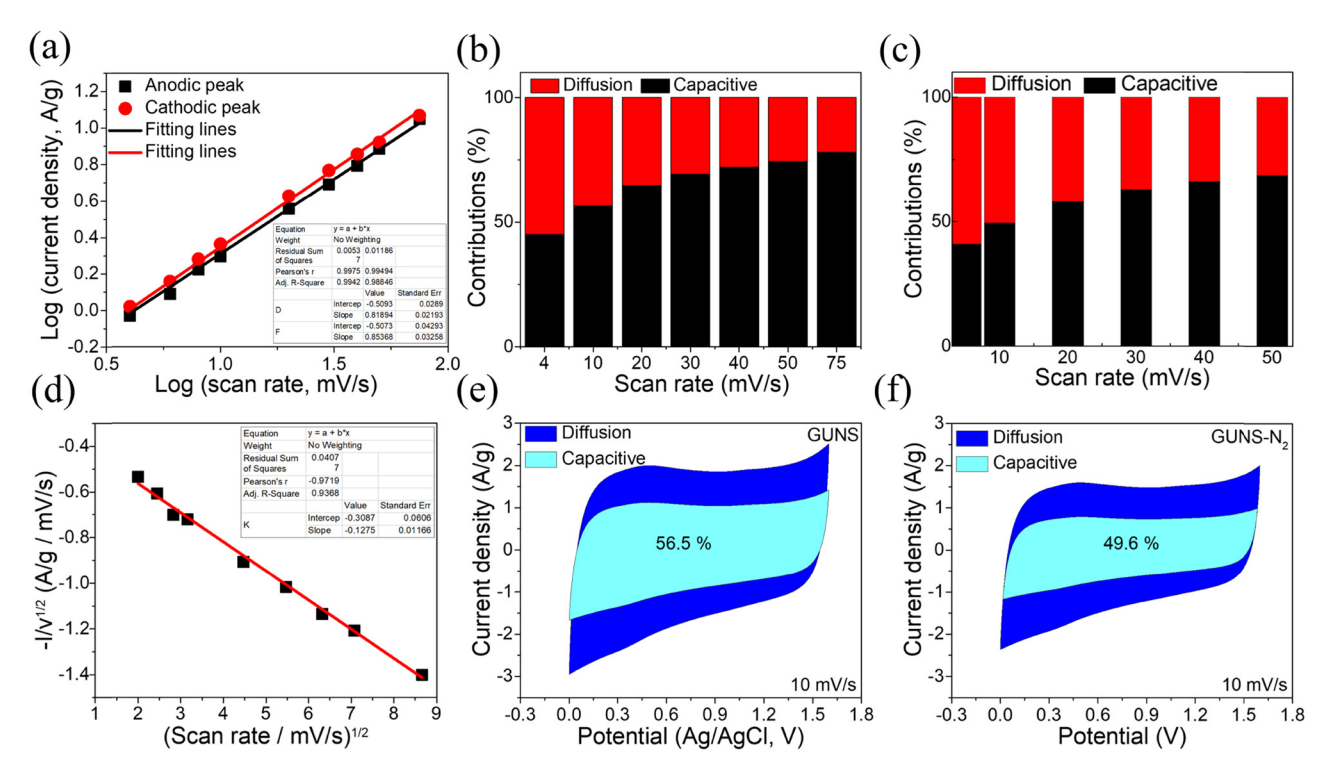


**Figure 7:** (a) Calculation of *b*-values; (b and c) capacitive/diffusion methods at different scan rates (4–75 mV/s) of GUNS and GUNS-N<sub>2</sub>; (d) calculation of  $k_1$  and  $k_2$  values; (e and f) capacitive/diffusion methods at 10 mV/s of GUNS and GUNS-N<sub>2</sub>.

$$i(V) = k_1(v) + k_2(v^{1/2}).$$
 (8)

In the above equation, i indicates total current,  $k_1(v)$  and  $k_2(v)^{1/2}$  are capacitive and diffusion-controlled based parameters of charge storage, respectively.  $k_1$  and  $k_1$  indicate arbitrary constants. Figure 7b and c depicts trends in capacitive behavior observed at different scan rates for GUNS and GUNS-N<sub>2</sub>. The slope and y-intercept of the plots can be used to calculate the values of  $k_1$  and  $k_2$  (Figure 7d). In addition, at 10 mV/s, the GUNS stores 56.5% of the total charge by the capacitance method and 43.5% by the diffusion control mechanism (Figure 7e). The capacitor of GUNS-N<sub>2</sub> stores 49.6% of the charge, and the diffusion control mechanism stores 50.4% (Figure 7f).

To examine the practical strength of the GUNSs//Zn device, the E and P of the device were computed. Figure 8 exhibits the Ragone plot. The GUNSs//Zn demonstrate specific energies of 64.88, 60, 57.33, 53.33, 49.77, and 46.66 W h/kg at 802.67, 1526.32, 2349.59, 4084.71, 5666.62, and 8270.12 W/kg. Furthermore, the current device outperforms several other previously explored SC and ZISC devices such as ZnCo<sub>2</sub>O<sub>4</sub>// AC (31.1 W h/kg, 759.9 W/kg) [36], Co@Co<sub>2</sub>O<sub>4</sub>//AC (38 W h/kg, 850 W/kg) [37], Zn-Ni-Al-Co//AC (36.5 W h/kg, 710 W/kg) [38], Zn foil//PDC (36.4 W h/kg, 376.6 W/kg) [39], MDC//Zn foam (36.4 W h/kg, 487.5 W/kg) [40], Zn//MXene-rGO (35.1 W h/kg, 278.8 kW/kg) [41], MXene/rGO//Zn (34.9 W h/kg at 279.9 W/kg) [42], and WC-6ZnN-12U//Zn@CC (27.7 W h/kg at 35.7 W/kg) [43]. These findings demonstrate the better performance of the GUNSs//Zn, including great cycle stability and exceptional specific energy. The main factor for the 2D GUNS material's outstanding characteristics is its beneficial 2D GUNS characteristics. As a result, 2D GUNSs have a reasonably large surface area and an unusually high electrochemical activity.

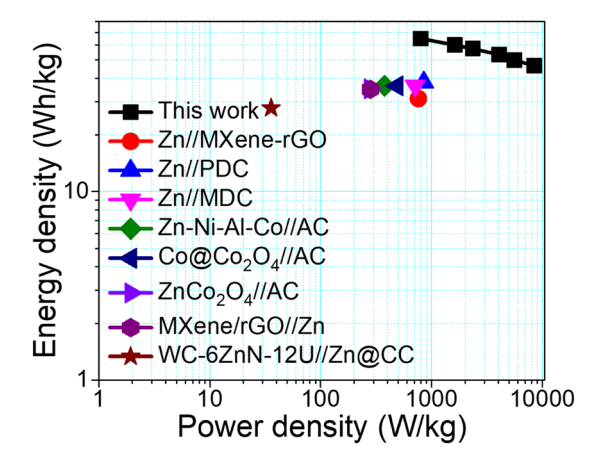


**Figure 8:** *E vs P* in the Ragone plot and comparison with previously explored SCs and ZISCs devices.

# 4 Conclusions

In conclusion, we have demonstrated a promising 2D GUNS cathode design for ZISCs. According to the experimental findings, the cathode material based on GUNSs exhibits a wide surface area and rapid charge transport. 2D GUNSs provide exceptional capacitance and specific energy during charging/discharging processes. The 2D GUNSs as a cathode was tested in three-electrode systems, and it provided an exceptionally high capacitance of 641 F/g at 1 A/g in an aqueous ZnSO<sub>4</sub> electrolyte, which is better than the GUNS-N<sub>2</sub> (462 F/g at 1 A/g) and pristine graphite (225.8 F/g at 1 A/g). When current density increases by a factor of 20 (20 A/g), the GUNS electrode still has an initial capacitance retention rate of 43.8%, which is much larger than that of the GUNS-N<sub>2</sub> (35.6%) and pristine graphite (8.4%) electrodes. Furthermore, a ZISC device was fabricated using GUNSs as cathode and Zn-foil as anode with 1 M ZnSO<sub>4</sub> electrolyte (denoted as GUNSs//Zn). In addition, extensive charge/discharge tests showed outstanding electrochemical stabilities; thus, the GUNSs//Zn device demonstrated an ultrahigh cyclic life of 10,000 cycles, and 96.76% of capacitance was maintained. Furthermore, GUNSs//Zn reveals a specific energy of 64.88 W h/kg at an ultrahigh specific power of 802.67 W/kg. This study paves the way for more investigation into 2D graphite materials for high-performance ZISCs.

**Funding information:** This work was financially supported by the Research Fund for International Scientists (grant number 52250410342) and the Supercomputing Center of Lanzhou University. This work was funded by the Researchers Supporting Project Number (RSPD2024R765) at King Saud University, Riyadh, Saudi Arabia.

**Author contributions:** All authors have accepted responsibility for the entire content of this manuscript and approved its submission.

**Conflict of interest:** The authors state no conflict of interest.

# References

- [1] Liu B, Wang X, Chen Y, Xie H, Zhao X, Nassr AB, et al. Honeycomb carbon obtained from coal liquefaction residual asphaltene for high-performance supercapacitors in ionic and organic liquidbased electrolytes. J Energy Storage. 2023;68:107826.
- [2] Sha L, Sui B, Wang P, Gong Z, Zhang Y, Wu Y, et al. 3D network of zinc powder woven into fibre filaments for dendrite-free zinc battery anodes. Chem Eng J. 2024;481:148393.

- [3] Huang Q, Jiang S, Wang Y, Jiang J, Chen Y, Xu J, et al. Highly active and durable triple conducting composite air electrode for low-temperature protonic ceramic fuel cells. Nano Res. 2023;16:9280-8.
- [4] Hao W, Xie J. Reducing diffusion-induced stress of bilayer electrode system by introducing pre-strain in lithium-ion battery. J Electrochem Energy Convers Storage. 2021;18(2):020909.
- Huang Z, Luo P, Wu Q, Zheng H. Constructing one-dimensional mesoporous carbon nanofibers loaded with NaTi2(PO4)3 nanodots as novel anodes for sodium energy storage. J Phys Chem Solids. 2022:161:110479.
- Mu S, Liu Q, Kidkhunthod P, Zhou X, Wang W, Tang Y. Molecular grafting towards high-fraction active nanodots implanted in N-doped carbon for sodium dual-ion batteries. Natl Sci Rev. 2020:8(7):nwaa178.
- Huang Z, Luo P, Zheng H, Lyu Z, Ma X. Novel one-dimensional V3S4@NC nanofibers for sodium-ion batteries. J Phys Chem Solids. 2023:172:111081.
- [8] Wang J, Zhang Y, Liu G, Zhang T, Zhang C, Zhang Y, et al. Improvements in the magnesium ion transport properties of graphene/CNT-wrapped TiO<sub>2</sub>-B nanoflowers by nickel doping. Small. 2024 Feb;20(6):2304969.
- Wang M, Jiang C, Zhang S, Song X, Tang Y, Cheng H-M. Reversible calcium alloying enables a practical room-temperature rechargeable calcium-ion battery with a high discharge voltage. Nat Chem. 2018;10:667-72.
- [10] Luo P, Huang Z, Lyu Z, Ma X. In-situ fabrication of a novel CNTspromoted Na3MnTi(PO4)3@C electrode in high-property sodiumion storage. J Phys Chem Solids. 2024;188:111911.
- [11] Zhang X, Tang Y, Zhang F, Lee C-S, Novel A. Aluminum-graphite dual-ion battery. Adv Energy Mater. 2016;6:1502588.
- [12] Chen C, Lee C-S, Tang Y. Fundamental understanding and optimization strategies for dual-ion batteries: a review. Nano-Micro Lett. 2023;15:121.
- [13] Zhu X, Xu Q, Li H, Liu M, Li Z, Yang K, et al. Fabrication of highperformance silver mesh for transparent glass heaters via electricfield-driven microscale 3D printing and UV-assisted microtransfer. Adv Mater. 2019;31(32):1902479.
- [14] Cai X, Shadike Z, Cai X, Li X, Luo L, An L, et al. Membrane electrode assembly design for lithium-mediated electrochemical nitrogen reduction. Energy Environ Sci. 2023;16:3063-73.
- [15] Sufyan Javed M, Zhang X, Ali S, Shoaib Ahmad Shah S, Ahmad A, Hussain I, et al. Boosting the energy storage performance of aqueous NH4 + symmetric supercapacitor based on the nanostructured molybdenum disulfide nanosheets. Chem Eng J. 2023;471:144486.
- [16] Javed MS, Najam T, Hussain I, Idrees M, Ahmad A, Imran M, et al. Fundamentals and scientific challenges in structural design of cathode materials for zinc-ion hybrid supercapacitors. Adv Energy Mater. 2022;53:2202303.
- [17] Javed MS, Asim S, Najam T, Khalid M, Hussain I, Ahmad A, et al. Recent progress in flexible Zn-ion hybrid supercapacitors: Fundamentals, fabrication designs, and applications. Carbon Energy. 2023;5(1):e271.
- [18] Javed MS, Mateen A, Ali S, Zhang X, Hussain I, Imran M, et al. The emergence of 2D MXenes based Zn-ion batteries: recent development and prospects. Small. 2022;18:2201989.
- [19] Zhao L, Fang H, Wang J, Nie F, Li R, Wang Y, et al. Ferroelectric artificial synapses for high-performance neuromorphic computing: Status, prospects, and challenges. Appl Phys Lett. 2024;124(3):30501.

- [20] Zhang W, Fu Q, Li J, Lian B, Xia Y, Zhou L, et al. Probing van der Waals magnetic surface and interface via circularly polarized X-rays. Appl Phys Rev. 2023;10(4):41308.
- [21] Gogotsi Y, Simon P. True performance metrics in electrochemical energy storage. Science. 2011;334:917-8.
- Jang B, Kim H, Park S-W, Lim M, Lee J, Go G-M, et al. In situ exfoliation and modification of graphite foil in supercapacitor devices: a facile strategy to fabricate high-performance supercapacitors. RSC Adv. 2021;11:4006-10.
- [23] Munuera J, Paredes J, Enterría M, Pagán A, Villar-Rodil S, Pereira M, et al. Electrochemical exfoliation of graphite in aqueous sodium halide electrolytes toward low oxygen content graphene for energy and environmental applications. ACS Appl Mater Interfaces. 2017:9:24085-99.
- [24] Wang Z, Fu W, Hu L, Zhao M, Guo T, Hrynsphan D, et al. Improvement of electron transfer efficiency during denitrification process by Fe-Pd/multi-walled carbon nanotubes: Possessed redox characteristics and secreted endogenous electron mediator. Sci Total Environ. 2021;781:146686.
- [25] Liu Q, Chen Q, Tang Y, Cheng H-M. Interfacial modification, electrode/solid-electrolyte engineering, and monolithic construction of solid-state batteries. Electrochem Energy Rev. 2023;6:15.
- Liu J, Yang H, Zhen SG, Poh CK, Chaurasia A, Luo J, et al. A green [26] approach to the synthesis of high-quality graphene oxide flakes via electrochemical exfoliation of pencil core. Rsc Adv. 2013;3:11745-50.
- [27] Xu P, Yuan Q, Ji W, Yu R, Wang F, Huo N. Study on the annealing phase transformation mechanism and electrochemical properties of carbon submicron fibers loaded with cobalt. Mater Express. 2022:12:1493-501.
- Liu M, Huang J, Meng H, Liu C, Chen Z, Yang H, et al. A novel approach to prepare graphite nanoplatelets exfoliated by three-roll milling in phenolic resin for low-carbon MgO-C refractories. | Eur Ceram Soc. 2023:43:4198-208.
- [29] Suk JW, Piner RD, An J, Ruoff RS. Mechanical properties of monolayer graphene oxide. ACS Nano. 2010;4:6557-64.
- [30] Liu Y, Qin J, Lu L, Xu J, Su X. Enhanced microwave absorption property of silver decorated biomass ordered porous carbon composite materials with frequency selective surface incorporation. Int I Miner Metall Mater. 2023:30:525-35.
- [31] Eckmann A, Felten A, Mishchenko A, Britnell L, Krupke R, Novoselov KS, et al. Probing the nature of defects in graphene by Raman spectroscopy. Nano Lett. 2012;12:3925-30.
- Huang X, Li S, Qi Z, Zhang W, Ye W, Fang Y. Low defect concentration few-layer graphene using a two-step electrochemical exfoliation. Nanotechnology. 2015;26:105602.
- Ye B, Kim J, Lee MJ, Chun SY, Jeong B, Kim T, et al. Mn-Ce oxide [33] nanoparticles supported on nitrogen-doped reduced graphene oxide as low-temperature catalysts for selective catalytic reduction of nitrogen oxides. Microporous Mesoporous Mater. 2021;310:110588.
- Zhang H, Chen Z, Zhang Y, Ma Z, Zhang Y, Bai L, et al. Boosting Znion adsorption in cross-linked N/P co-incorporated porous carbon nanosheets for the zinc-ion hybrid capacitor. J Mater Chem A. 2021;9:16565-74.
- Bhoyate S, Ranaweera CK, Zhang C, Morey T, Hyatt M, Kahol PK, et al. Eco-friendly and high performance supercapacitors for elevated temperature applications using recycled tea leaves. Glob Chall. 2017;1:1700063.

- [36] Javed MS, Khan AJ, Ahmad A, Siyal SH, Akram S, Zhao G, et al.

  Design and fabrication of bimetallic oxide nanonest-like structure/
  carbon cloth composite electrode for supercapacitors. Ceram Int.
  2021;47:30747–55.
- [37] Zhao X, Fan B, Qiao N, Soomro RA, Zhang R, Xu B. Stabilized Ti3C2Tx-doped 3D vesicle polypyrrole coating for efficient protection toward copper in artificial seawater. Appl Surf Sci. 2024;642:158639.
- [38] Cai X, Li X, You J, Yang F, Shadike Z, Qin S, et al. Lithium-mediated ammonia electrosynthesis with ether-based electrolytes. J Am Chem Soc. 2023;145(47):25716–25.
- [39] Wang S, Liu Y, He L, Sun Y, Huang Q, Xu S, et al. A gel polymer electrolyte based on IL@NH2-MIL-53 (Al) for high-performance allsolid-state lithium metal batteries. Chin J Chem Eng. 2024.
- [40] Zhang Q, Zhao B, Wang J, Qu C, Sun H, Zhang K, et al. High-performance hybrid supercapacitors based on self-supported 3D ultrathin porous quaternary Zn-Ni-Al-Co oxide nanosheets. Nano Energy. 2016;28:475–85.
- [41] Zeng S, Shi X, Zheng D, Yao C, Wang F, Xu W, et al. Molten salt assisted synthesis of pitch derived carbon for Zn ion hybrid supercapacitors. Mater Res Bull. 2021;135:111134.
- [42] Xiong T, Shen Y, Lee WSV, Xue J. Metal Organic framework derived carbon for ultrahigh power and long cyclic life aqueous Zn ion capacitor. Nano Mater Sci. 2020;2:159–63.
- [43] Wang Q, Wang S, Guo X, Ruan L, Wei N, Ma Y, et al. Mxenereduced graphene oxide aerogel for aqueous zinc-ion hybrid supercapacitor with ultralong cycle life. Adv Electron Mater. 2019;5:1900537.